Supplementary Information

Regulating Solvation Structure with N,N-Dimethylacetamide Co-solvent for High-Performance Zinc-ion Batteries

Mingyan Li,[1,2] *Xiang Feng,*[1] *Junyi Yin,*[1] *Tianyi Cui,*[3] *Fuxiang Li,*[1] *Jingzhe Chen,*[1] *Yuyao Lin,*[4] *Xin Xu,*[1,*] *Shujiang Ding,*[2,5,*] *Jianhua Wang* [1,*]

[1]State Key Laboratory of Electrical Insulation and Power Equipment, School of Electrical Engineering, Xi'an Jiaotong University, Xi'an 710049, P.R. China

[2]Xi'an Key Laboratory of Sustainable Energy Materials Chemistry, School of Chemistry, Xi'an Jiaotong University, Xi'an, 710049, P.R. China

[3]China Power Complete Equipment Co.,Ltd, Beijing 100080, P.R. China

[4]Department of Plastic, Aesthetic and Maxillofacial Surgery, The First Affiliated Hospital of Xi'an Jiaotong University, Xi'an 710061, P.R. China

[5]Engineering Research Center of Energy Storage Materials and Devices, Ministry of Education, P.R. China

Corresponding Author

*E-mail: xu.xin@xjtu.edu.cn (Xin Xu); dingsj@mail.xjtu.edu.cn (Shujiang Ding); jhwang@mail.xjtu.edu.cn (Jianhua Wang).

1. Experimental Section

Preparation of the Electrolyte: The optimized electrolyte (DMA*x*, *x*=0, 5, 10, 20, 30) was prepared by adding 5.7512 g of $ZnSO_4 \cdot 7H_2O$ (98%, Aladdin) into a mixed solution of *x* ml of N,N-Dimethylacetamide (99.8%, Aladdin) and 100-*x* ml of deionized (DI) water.

Synthesis of cathode materials: The $NH_4V_4O_{10}$ powders were synthesized by a hydrothermal method. In detail, 0.585 g of ammonium vanadate (NH_4VO_3, Aladdin, 99%) was added into 35 mL DI water. Then 0.9455 g oxalic acid ($H_2C_2O_4 \cdot 2H_2O$, Meryer, 99%) powders were added into the NH_4VO_3 solution under magnetically stirring. The solution was transferred to a 50 mL Teflon-lined autoclave and heated at 140 °C for 12 h. After cooling, the products were collected and washed with DI water, then dried at 70 °C overnight to finally obtain the $NH_4V_4O_{10}$ powders.

***Characterizations*:** The morphologies and structures of the samples were characterized by field-emission scanning electron microscopy (FESEM; GeminiSEM 500). X-ray diffraction (XRD) patterns were recorded with a X-ray diffractometer using Cu-Kα1 radiation (λ=1.54184 Å) from 5° to 90°.

***Electrochemical Measurements*:** The slurry was prepared by mixing as-prepared active materials, super P, and polyvinylidene fluoride (PVDF) in a mass ratio of 7: 2: 1 with certain amounts of N-methyl-2-pyrrolidone (NMP). Then the working electrode was prepared by coating the slurry on the stainless foil and was dried at 80 °C under vacuum for 12 h. The mass loading of the $NH_4V_4O_{10}$ materials in coin cell were about 2 mg cm^{-2}. The Zn//Zn symmetric cells and full cells for electrochemical tests were

fabricated by assembling CR2025 coin cells in air, employing thin Zn foil (100μm) as anode and glass microfiber (Whatman) as the separator. 80 μl of electrolytes were added to each coin cell. The electrochemical performance of the batteries in this work was evaluated using CR2025 coin cells on a NEWARE CT-4008T battery test system. Electrochemical impedance spectroscopy (EIS) was performed on an electrochemical workstation (CHI660E) within the frequency range from 10^5 to 10^{-2} Hz. Cyclic voltammetry curves test, Linear polarization measurements and Tafel curves test were carried out on the same electrochemical workstation.

Computional Simulations: Molecular dynamics (MD) simulations are carried out with Gromacs version 2019.6. Initial simulation systems are constructed by uniformly dispersing 50 Zn^{2+}, 50 SO_4^{2-} into solvent environment, which is a mixture of 54 DMA molecules and 1111 water molecules, or pure water consisting of 1389 water molecules. OPC model[1] is used to describe water. For Zn^{2+}, the parameters compatible with OPC water model proposed by Merz et al.[2] are adopted. Parameters proposed by Christopher et al. are adopted for SO_4^{2-}[3]. GAFF force field[4] is used for DMA. Coulombic interactions are computed with the particle mesh Ewald algorithm. Lennard Jones (LJ) potential with a truncation value of 1.2 nm is used to compute vdW interactions. LJ parameters between unlike atoms are derived by Lorentz-Berthelot mixing rules. Initial conformations are energy-minimized, then 50-ns MD runs are carried out at 298.15 K and 1 bar. A time step of 1 fs is used to integrate the motion equations. Three-dimensional periodic boundary conditions are applied during simulations.

Electronic structure of the solvation structures of Zn^{2+} is calculated at the B3LYP-

D3/def2-TZVP level of theory with Gaussian 16 software package. Electrostatic potential and electron density are analyzed by Multiwfn program version 3.8-dev[5], and the ESP-mapped molecular surface is visualized with VMD version 1.9.3[6].

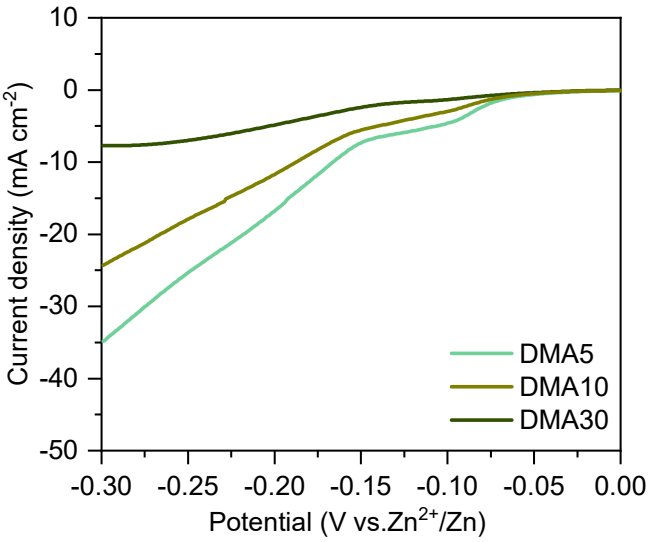

Figure S1. LSV curves for Zn electrodes in different electrolytes.

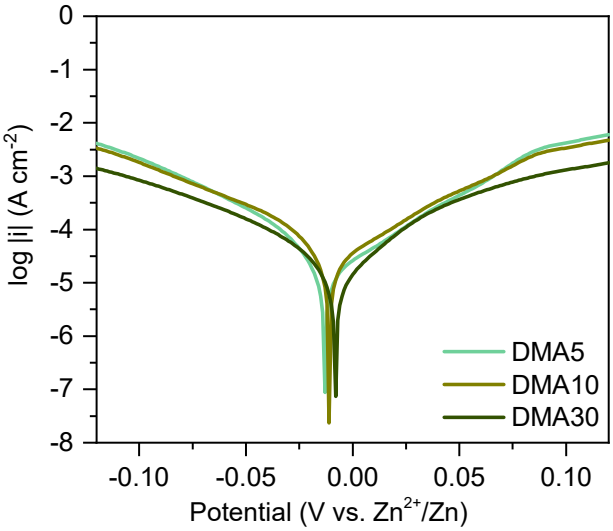

Figure S2. Tafel curves for Zn electrodes in different electrolytes.

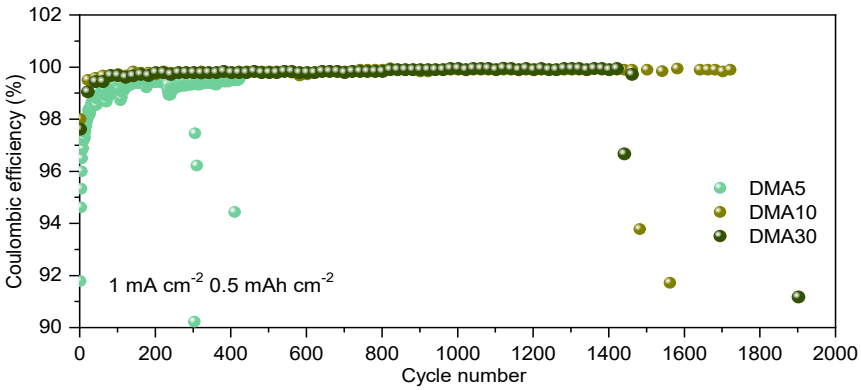

Figure S3. Coulombic efficiency measurements of Cu//Zn asymmetric cells with different electrolytes.

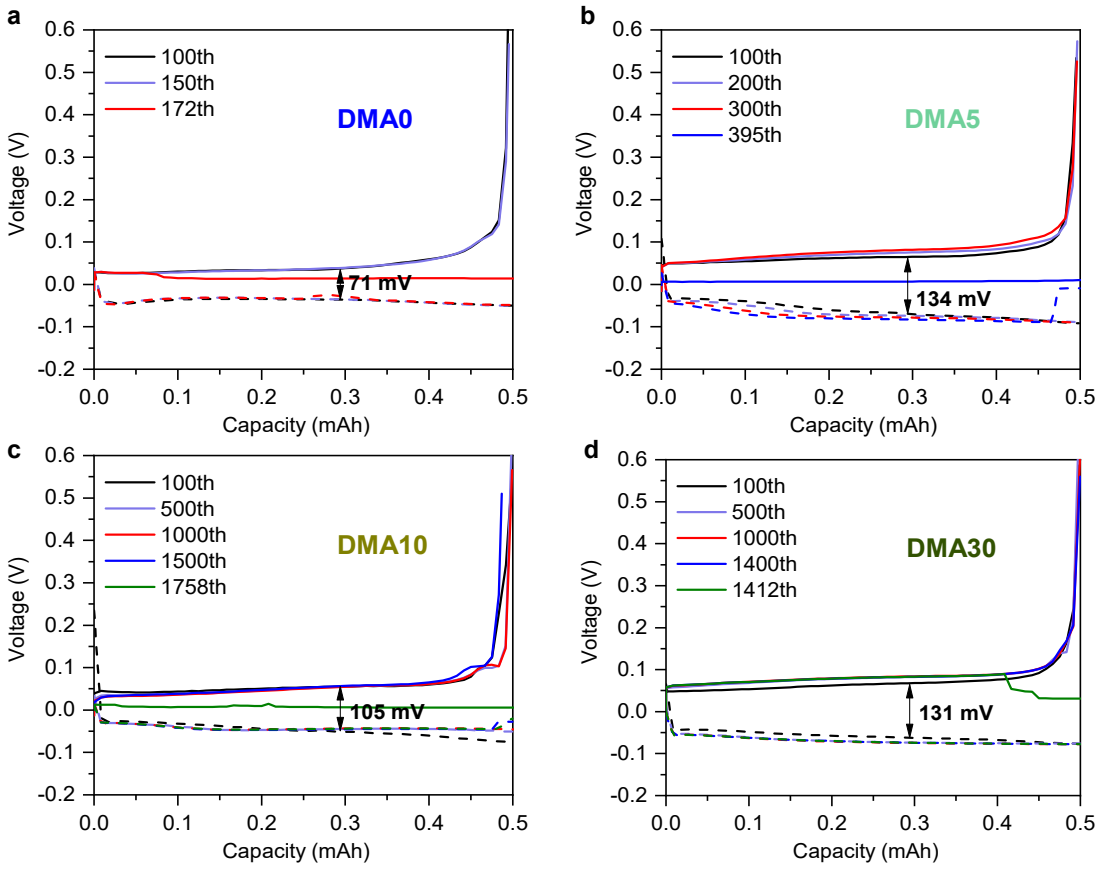

Figure S4. Corresponding voltage profiles of Cu//Zn asymmetric cells in different electrolytes (DMA0, DMA5, DMA10, and DMA30).

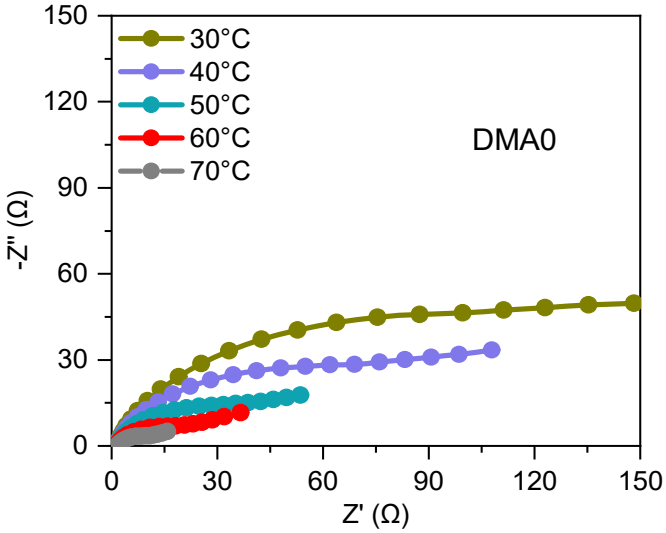

Figure S5. EIS plots of the Zn//Zn symmetric cells with DMA0 electrolyte at different temperatures.

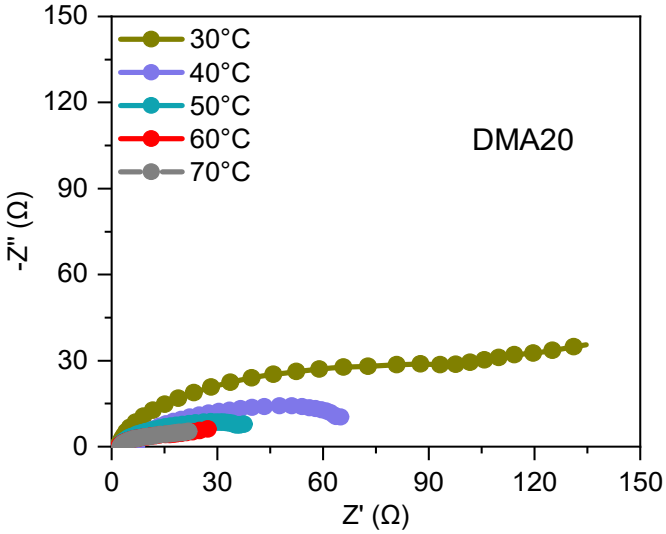

Figure S6. EIS plots of the Zn//Zn symmetric cells with DMA20 electrolyte at different temperatures.

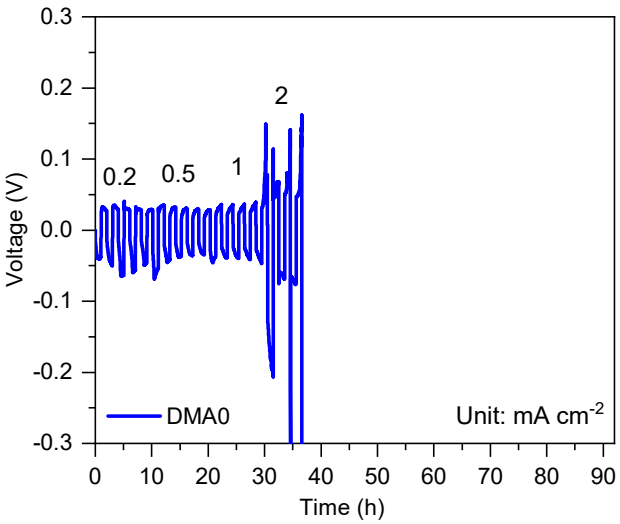

Figure S7. Rate performance of Zn//Zn symmetric cells with the DMA0 electrolyte.

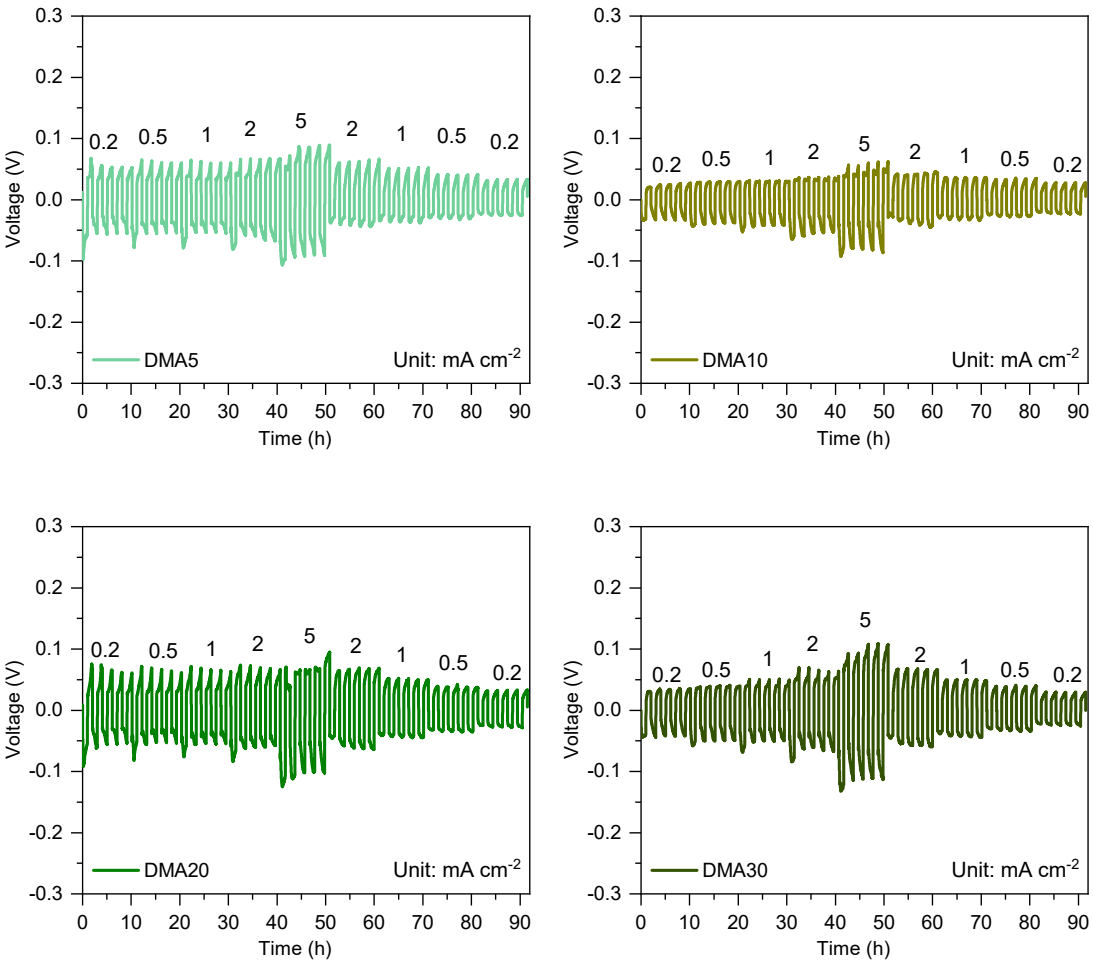

Figure S8. Rate performance of Zn//Zn symmetric cells with different electrolytes from 0.2 to 5 mA cm^{-2}.

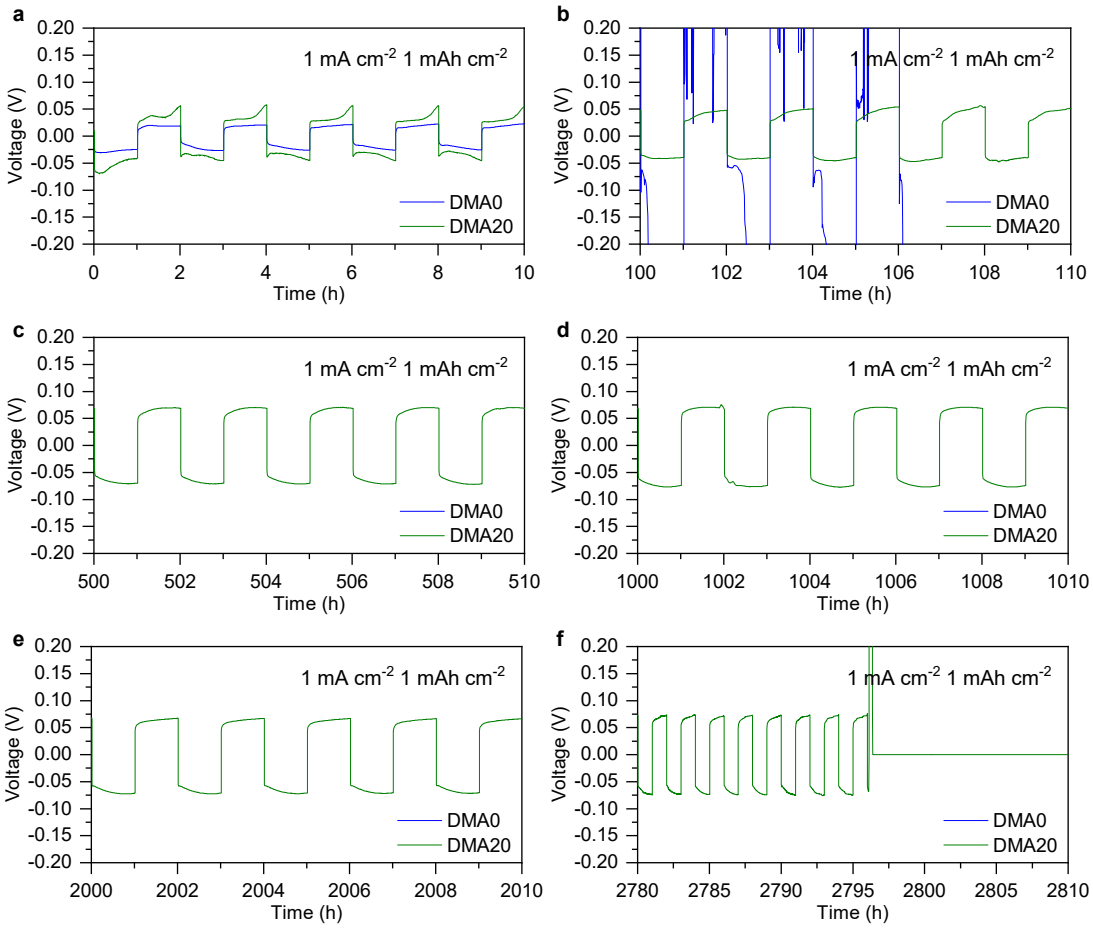

Figure S9. The local enlargement of the voltage-time curves. (a) 0-10 h; (b) 100-110 h; (c) 500-510 h; (d) 1000-1010 h; (e) 2000-2010 h; (f) 2780-2810 h. The symmetric cell with DMA20 electrolyte eventually exhibited clear signs of a short-circuit failure.

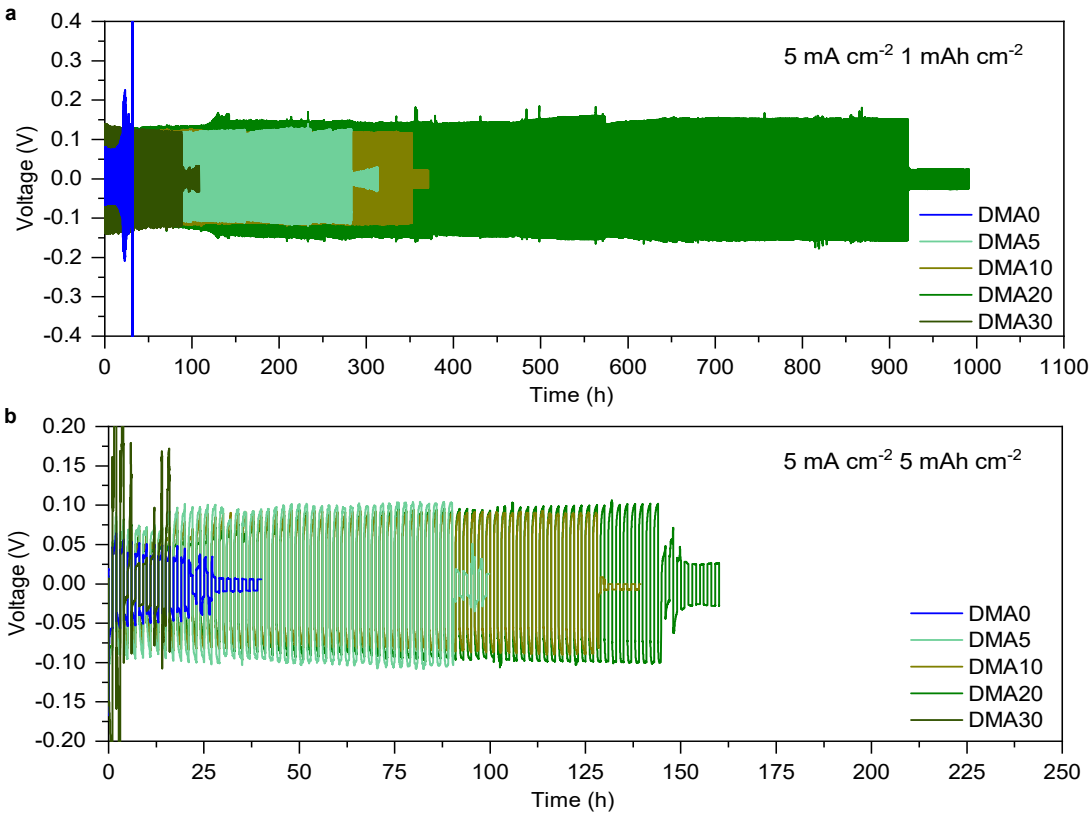

Figure S10. Cycle performance of symmetric cells with different electrolytes at (a) 5 mA cm^{-2}, 1 mAh cm^{-2} and (b) 5 mA cm^{-2}, 5 mAh cm^{-2}.

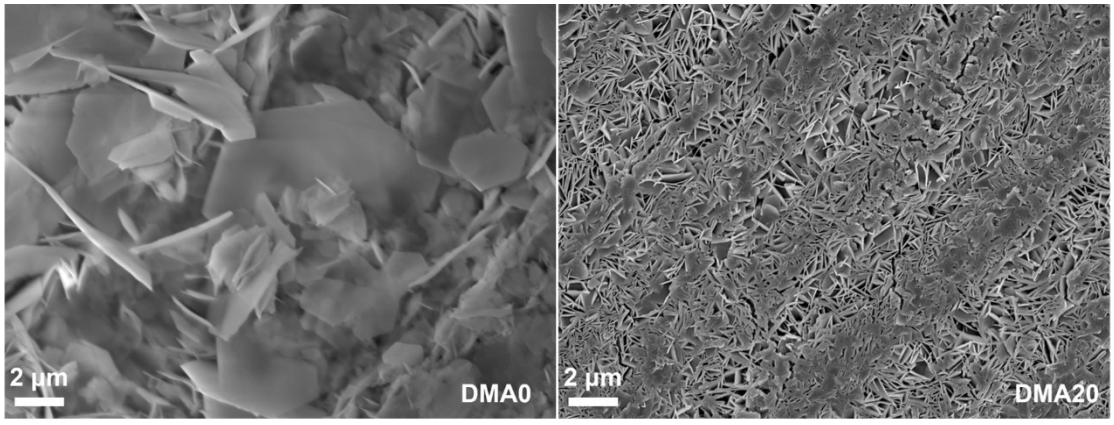

Figure S11. SEM images of Zn electrodes stripped from the Zn//Zn symmetric cells with DMA0 electrolyte and DMA20 electrolyte after cycling for 10 cycles (1 mA cm^{-2}, 1 mAh cm^{-2}).

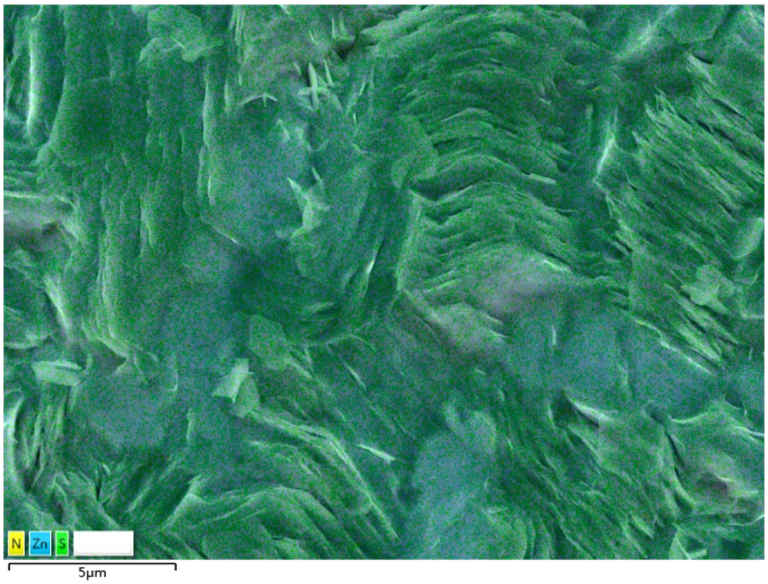

Figure S12 Distribution of Zn, N and S elements on the zinc electrode surface (after 10 cycles under conditions of 5 mA cm^{-2} and 5 mAh cm^{-2} in DMA20 electrolyte). The presence of N and some O might originate from chemical adsorption due to the characteristics of DMA molecules. The S element corresponds to by-products (ZHS). Firstly, the uniform hexagonal deposits as a whole are not ZHS but should be the zinc plate, as their central region lacks S element. A small amount of by-products (S: 3.22 wt%) can be observed at the edge tips of the zinc plate. This confirms the phenomenon of uniform zinc deposition on the zinc anode, dispelling the illusion caused by hexagonal ZHS structures resembling the zinc plate.

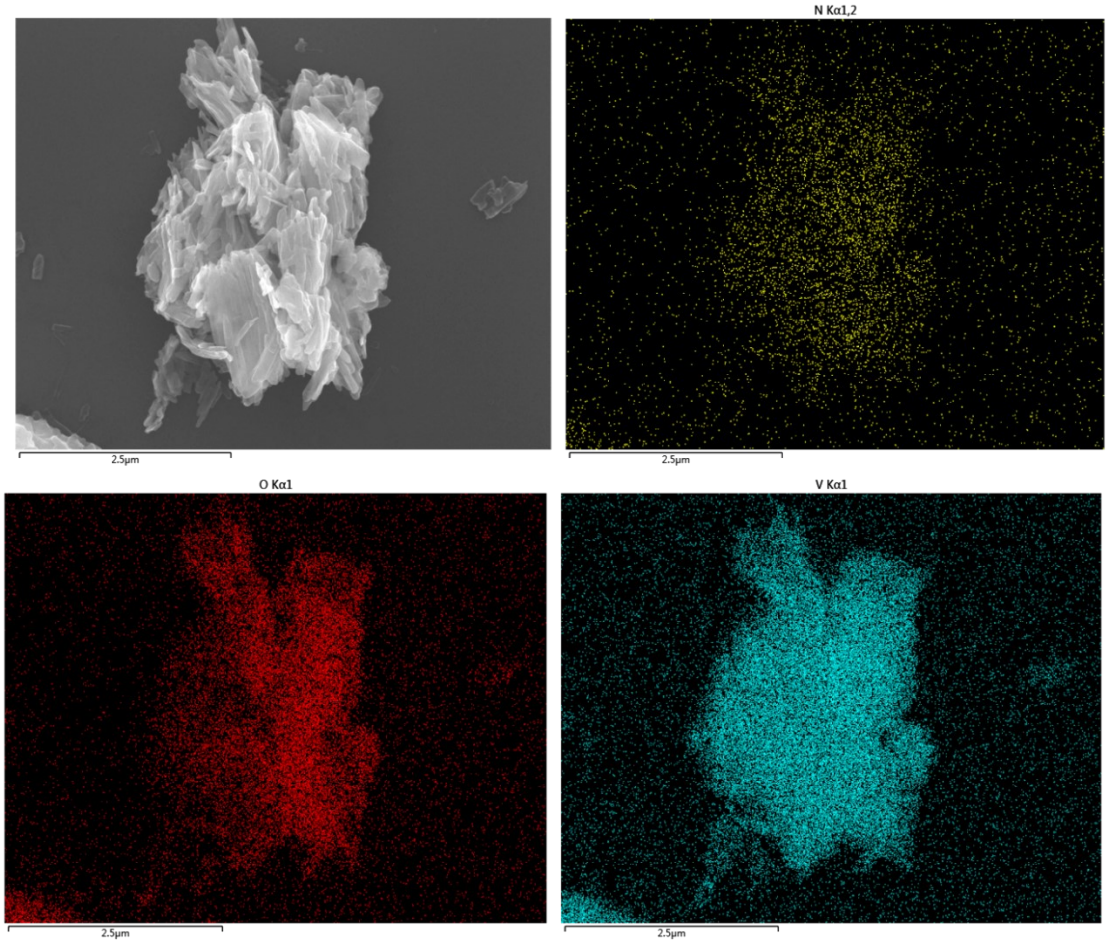

Figure S13. SEM image and EDS mapping of $NH_4V_4O_{10}$ powders.Scale bar: 2.5 μm.

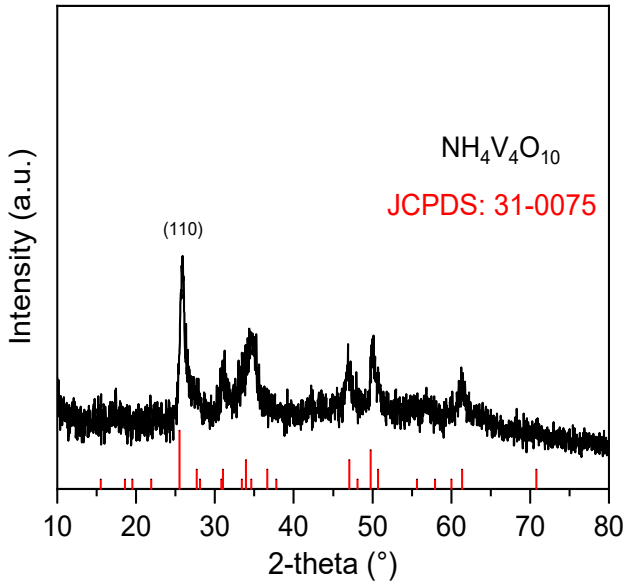

Figure S14. XRD pattern of $NH_4V_4O_{10}$ powders.

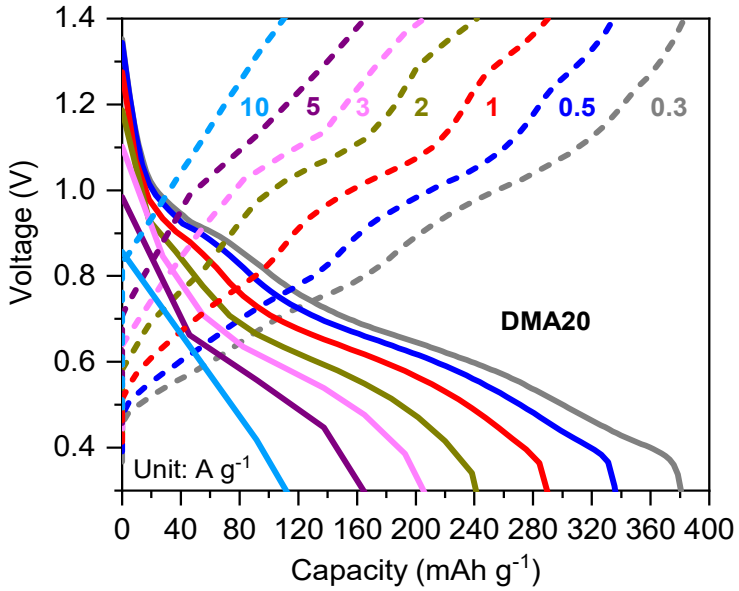

Figure S15. Charge–discharge curves of $NH_4V_4O_{10}$//Zn full cell with DMA20 electrolyte at different current densities.

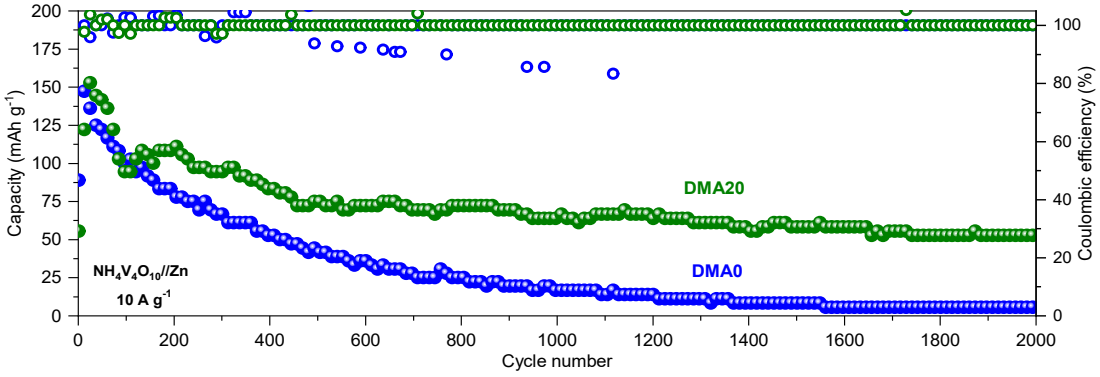

Figure S16. Long-term cycling performance of $NH_4V_4O_{10}$//Zn full-cell at 10 A g^{-1} in different electrolytes.

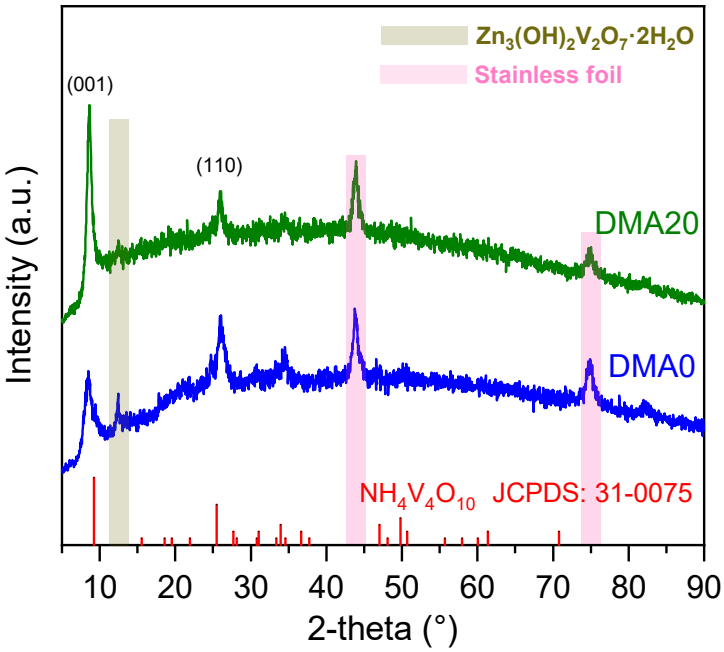

Figure S17. XRD spectra of $NH_4V_4O_{10}$ cathodes after 100 cycles (3 A g^{-1}) in DMA0 and DMA20 electrolytes.

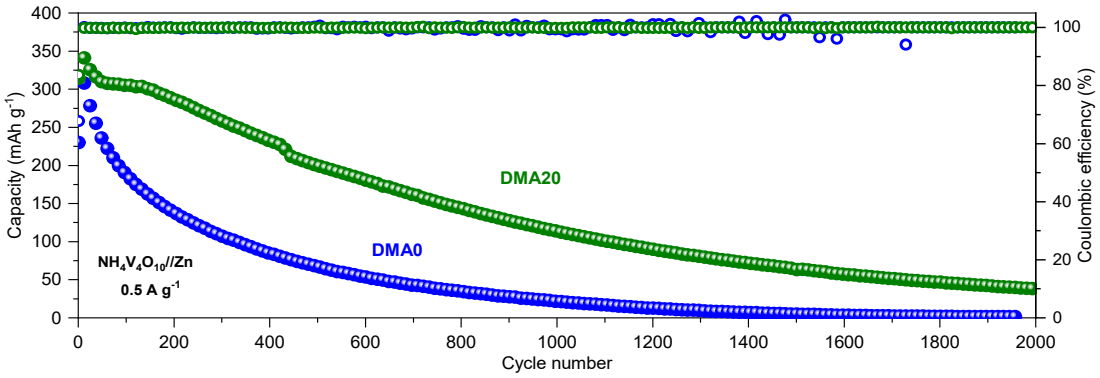

Figure S18. Long-term cycling performance of $NH_4V_4O_{10}$//Zn full-cell at 0.5 A g^{-1} in different electrolytes.

Table S1 The ionic conductivity of different electrolytes.

	DMA0	DMA5	DMA10	DMA20	DMA30
Ionic conductivity (mS cm^{-1})	54.9	43.0	33.3	28.6	17.3

Table S2 Contents of Zn, S, N, and O

	Zn	S	N	O
Mass fraction/ wt.%	89.34	3.22	0.27	7.17

Reference

1. S. Izadi, R. Anandakrishnan and A. V. Onufriev, *The Journal of Physical Chemistry Letters*, 2014, **5**, 3863-3871.
2. Z. Li, L. F. Song, P. Li and K. M. Merz, *J. Chem. Theory Comput.*, 2020, **16**, 4429-4442.
3. C. D. Williams and P. Carbone, *The Journal of Chemical Physics*, 2015, **143**, 174502.
4. J. Wang, R. M. Wolf, J. W. Caldwell, P. A. Kollman and D. A. Case, *J. Comput. Chem.*, 2004, **25**, 1157-1174.
5. T. Lu and F. Chen, *J. Comput. Chem.*, 2012, **33**, 580-592.
6. W. Humphrey, A. Dalke and K. Schulten, *J. Mol. Graphics*, 1996, **14**, 33-38.